
# Tailoring of ion species composition in complex plasmas with charge exchange collisions

K. Ostrikov

Citation: Physics of Plasmas (1994-present) **12**, 062105 (2005); doi: 10.1063/1.1925547
View online: http://dx.doi.org/10.1063/1.1925547
View Table of Contents: http://scitation.aip.org/content/aip/journal/pop/12/6?ver=pdfcov
Published by the AIP Publishing



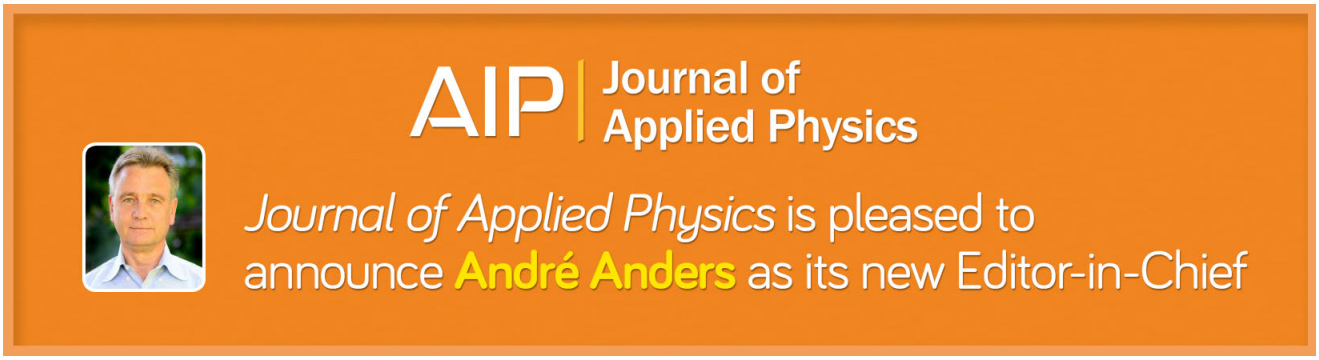

# Tailoring of ion species composition in complex plasmas with charge exchange collisions

K. Ostrikov[a)]
*School of Physics, The University of Sydney, Sydney, New South Wales 2006, Australia*

(Received 17 January 2005; accepted 12 April 2005; published online 26 May 2005)

A generic approach towards tailoring of ion species composition in reactive plasmas used for nanofabrication of various functional nanofilms and nanoassemblies, based on a simplified model of a parallel-plate rf discharge, is proposed. The model includes an idealized reactive plasma containing two neutral and two ionic species interacting via charge exchange collisions in the presence of a microdispersed solid component. It is shown that the number densities of the desired ionic species can be efficiently managed by adjusting the dilution of the working gas in a buffer gas, rates of electron impact ionization, losses of plasma species on the discharge walls, and surfaces of fine particles, charge exchange rates, and efficiency of three-body recombination processes in the plasma bulk. The results are relevant to the plasma-aided nanomanufacturing of ordered patterns of carbon nanotip and nanopyramid microemitters. © *2005 American Institute of Physics*.
[DOI: 10.1063/1.1925547]

## I. INTRODUCTION

Tailoring of reactive ionized gas systems is currently one of the most critical problems in plasma-aided industrial materials processing, microelectronic manufacturing, environmental remediation, and some other areas.[1–3] In particular, fabrication of various nanoscale assemblies, functional nanofilms, and advanced nanodevices requires precise management of composition, fluxes, and energetic states of specific reactive species that serve a certain purpose.[4–7] Some species can serve as energetic projectiles that clean substrates from unwelcome residues, while the other ones can be used to activate the deposition surface, and yet other ones can be regarded as building blocks that land on the surface and incorporate into the assembly of film being grown.[7–9] For example, low-temperature plasmas of $H_2+CH_4/C_2H_2$ gas mixtures diluted in argon have been widely used for nanofabrication of single crystalline carbon microemitters, carbon nanofibers, nanotubes, nanopyramids, and other functional structures.[10–15] It is notable that every process stage usually requires elevated abundance of certain ionic and radical plasma species.

Manufacturing of carbon microemitters in plasmas of gas mixtures of argon, hydrogen, and hydrocarbon gas feedstock is just an example in a virtually infinite continuum of applications of low-temperature plasmas, where controlled and selective species production and manipulation is a key strategy for success.[1–3,16] From the general practical point of view, the plasma parameters need to be managed (in every process during each specific stage) to ensure higher number densities of the desired [e.g., atomic hydrogen during the surface activation stage and carbon-bearing cation building units during the carbon nanostructure (CNS) assembly stage[13–15]] plasma species.

However, due to a large number of discharge control parameters and overwhelming complexity of the plasma chemistry in reactive gases used for nanofabrication and other applications, it is very difficult to work out a generic recipe for the optimized species production. In particular, the equilibrium plasma composition is usually very strongly affected by intense collisions between numerous plasma species. Nonetheless, simple plasma models can enable one to predict the optimal ranges of operation parameters to maximize the number densities of the species in question. Even though modeling of multicomponent plasmas in complex gas mixtures is a common and advanced topic nowadays,[17–20] a focused modeling of specific features of plasma discharges and tailoring of the required nanofabrication species have not attracted the attention they merit.

Here, by using a simple model of an idealized rf complex plasma discharge with two neutral, two ionic species, and a low-density fine solid particle component, we will show that the number densities of the required ionic species can be controlled by managing the partial pressures (neutral densities) of the working gas and the diluent (buffer gas), as well as relative rates of the ionic species creation (via electron impact ionization and charge exchange collisions) and loss in the plasma bulk (through three-body recombination and charge exchange collisions) and on solid surfaces (chamber walls/electrodes and microdispersed fine particles).

The paper is organized as follows. In Sec. II, the problem is formulated and a basic set of equations is given. In Sec. III, the simplified model of species balance in the discharge is introduced and the equilibrium number density of electrons is derived. Section IV is devoted to the numerical analysis of relative concentrations of the "working" and "buffer" ionic species composition. Applications of the results for tailoring of ionized gas systems for various plasma applications for the synthesis of advanced materials and development of nanoscale devices, as well as the limitations of the current model, are discussed in Sec. V. The paper con-

[a)]Also with Plasma Sources and Applications Center, NIE, Nanyang Technological University, 637616, Singapore. Electronic mail: K.Ostrikov@physics.usyd.edu.au

 

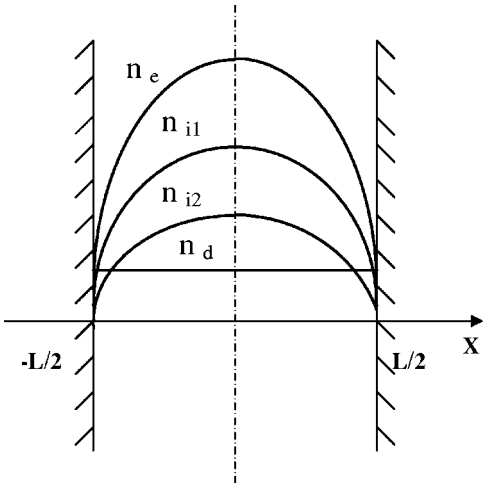


FIG. 1. Schematic representation of a two-ion species plasma with a small proportion of fine solid particles in a parallel-plate rf discharge geometry.

cludes with a summary of the results obtained and a brief outlook for future research in this direction.

## II. FORMULATION AND MAIN EQUATIONS

We consider a one-dimensional model of the plasma column representative to common parallel-plate discharge configurations. A schematics of the parallel-plate discharge of our interest here is depicted in Fig. 1. Two large-area electrodes, with linear dimensions in $y$ and $z$ directions much exceeding the interelectrode gap $L$, are located at $x=\pm L/2$. On the other hand, $L \gg \lambda_{\mathrm{mfp}}^{jk}$, where $\lambda_{\mathrm{mfp}}^{jk}$ is the mean free path of species $j$ in collisions with species $k$. An idealized reactive plasma discharge contains two neutral and two ionic species, as well as a microdispersed solid phase uniformly distributed over the plasma bulk. The number densities of the plasma species are nonuniform along the $x$ direction, whereas the electron and ion temperatures are assumed uniform in the plasma slab as schematically shown in Fig. 1. Such assumptions are common in the modeling of parallel-plate rf discharges[21] and are representative to experimentally measured spatial profiles of the main plasma parameters in this type of the plasma discharges.[16] For clarity, the working ionic and neutral species are denoted by subscript 1, while the buffer species by subscript 2.

The microdispersed solid phase comprises solid spherical nanoparticles of the radius $a_p$ and number density $n_p$. The particle size, which is typically 10–100 nm in the CNSs nanofabrication experiments, is smaller than $\lambda_{\mathrm{mfp}}^{jk}$ and the plasma Debye length $\lambda_D$. Their charge is assumed fixed and the details of fine particle charging and charge fluctuations are not considered here. The two neutral and two singly charged positive ionic species interact and continuously transform into each other through charge exchange collisions. It is thus assumed that both the ion species are generated through the electron impact ionization and charge exchange collisions, whereas more complex collisions between heavy species (such as dissociation, atom abstraction, Penning ionization, etc.) are neglected. The charged species disappear through three separate channels: ambipolar diffusion losses to the discharge walls, species collection by fine solid particles, and three-body recombination in the plasma bulk. Any specific details of rf power balance required for the study of the discharge maintenance, as well as any near-electrode effects are not considered here. Taking into account that the plasma is overly charge neutral and contains singly charged ions $i1$ and $i2$, electrons, and fine particles, one can write down the overall charge balance in the discharge $n_{i1}+n_{i2}=n_e+\Sigma_k n_d^k Z_d^k$, where $n_j$ is the number density of the $j$th species ($j=e,i1,i2$), and $n_d^k$ and $Z_d^k$ are the number density and charge of fine particles in a specific charging state $k$. In this model, plasma species losses on fine particles are introduced in a simplified manner by setting a fraction of the species loss due to collection by fine particles to the total species loss in the plasma as a parameter in computations. Other multiple species that are usually present in multicomponent processing plasmas are not considered here.

In this geometry, the number densities of the plasma species can be obtained from the following set of particle balance equations:

$$\frac{\partial \Gamma_e}{\partial x} = \nu_{\mathrm{ion}}^{\mathrm{eff}} n_e - \nu_{ed} n_e - (\rho_{1e} n_{i1} + \rho_{2e} n_{i2}) n_e^2 \quad \text{for electrons,} \tag{1}$$

$$\frac{\partial \Gamma_{i1}}{\partial x} = \nu_{\mathrm{ion}}^{(1)} n_e - \nu_{id}^{(1)} n_{i1} - \nu_{\mathrm{ex}}^{(1)} n_{i1} + \nu_{\mathrm{ex}}^{(2)} n_{i2} - \rho_{1e} n_{i1} n_e^2 \quad \text{for ionic species 1,} \tag{2}$$

$$\frac{\partial \Gamma_{i2}}{\partial x} = \nu_{\mathrm{ion}}^{(2)} n_e - \nu_{id}^{(2)} n_{i2} - \nu_{\mathrm{ex}}^{(2)} n_{i2} + \nu_{\mathrm{ex}}^{(1)} n_{i1} - \rho_{2e} n_{i2} n_e^2 \tag{3}$$

for ionic species 2, where $\Gamma_j = n_j v_j$, $n_j$, and $v_j$ are the flux, number density, and fluid velocity of the $j$th ($j=e$, $i1$, and $i2$) plasma species, respectively; $\nu_{\mathrm{ion}}^{\mathrm{eff}} = \nu_{\mathrm{ion}}^{(1)} + \nu_{\mathrm{ion}}^{(2)}$, $\nu_{\mathrm{ion}}^{(1)} = \alpha_{\mathrm{ion}}^{(1)} N_{n1}$, and $\nu_{\mathrm{ion}}^{(2)} = \alpha_{\mathrm{ion}}^{(2)} N_{n2}$ are the ionization rates of the first and the second ionic species, $\alpha_{\mathrm{ion}}^{(1)} = \alpha_{\mathrm{ion}}^{(10)} \exp(-U_{\mathrm{ion}}^{(1)}/T_e)$ and $\alpha_{\mathrm{ion}}^{(2)} = \alpha_{\mathrm{ion}}^{(20)} \exp(-U_{\mathrm{ion}}^{(2)}/T_e)$, $U_{\mathrm{ion}}^{(1)}$ and $U_{\mathrm{ion}}^{(2)}$ are the ionization potentials, $T_e$ is the effective electron temperature, and $N_{n1}$, $N_{n2}$ are the densities of neutral species $n1$ and $n2$. In the case of arbitrary electron energy distribution function, $T_e = 2/3\langle \mathcal{E} \rangle$, where $\langle \mathcal{E} \rangle$ is the averaged electron energy.

In Eqs. (1)–(3), $\nu_{\mathrm{ex}}^{(1)} = \alpha_{\mathrm{ex}}^{(1)} N_{n2}$ and $\nu_{\mathrm{ex}}^{(2)} = \alpha_{\mathrm{ex}}^{(2)} N_{n1}$ denote the rates of charge exchange collisions between the relevant ionic and neutral species,

$$i1^+ + n2 \rightarrow n1 + i2^+$$

with the reaction rate $\nu_{\mathrm{ex}}^{(1)}$ and

$$i2^+ + n1 \rightarrow n2 + i1^+$$

with the reaction rate $\nu_{\mathrm{ex}}^{(2)}$. For the sake of simplicity and because of the limited number of species in the model, charge exchange collisions were chosen as representative to a large variety of collisions between ionic and radical/nonradical neutral species in the discharge. We consider weakly ionized plasmas, where the dominant types of ion collisions are normally inelastic charge exchange and elastic ion-neutral collisions.[22,23] In charge exchange collisions, an

electron is transferred from a neutral to an ion, without any exchange of momentum, i.e., a fast incoming ion is replaced by a slow neutral.[22,23] We recall that slow neutrals are beneficial for the efficient interaction with the deposition surface during the surface activation and nanoassembly process stages.[13–15]

In Eqs. (1) and (2), terms $\partial\Gamma_j/\partial x$ describe diffusion losses of the $j$th plasma species to the discharge walls, where

$$\Gamma_e = -\mu_e n_e E - D_e(\partial n_e/\partial x), \tag{4}$$

$$\Gamma_{i1} = \mu_{i1} n_{i1} E - D_{i1}(\partial n_{i1}/\partial x), \tag{5}$$

and

$$\Gamma_{i2} = \mu_{i2} n_{i2} E - D_{i2}(\partial n_{i2}/\partial x) \tag{6}$$

are the equilibrium fluxes of the plasma species to the discharge walls, where $D_j = T_j/m_j\nu_{jn}$, $\mu_j = e/m_j\nu_{jn}$, $T_j$, and $m_j$ are the diffusion and mobility coefficients, temperatures, and masses of the $j$th($j=e,i1,i2$) species, respectively. The effective rates of the electron- and ion-neutral collisions are $\nu_{en} = V_{Te}(N_{n1}\sigma_{en1} + N_{n2}\sigma_{en2})$, $\nu_{i1n} = v_{i1}(N_{n1}\sigma_{i1n1} + N_{n2}\sigma_{i1n2})$, and $\nu_{i2n} = v_{i2}(N_{n1}\sigma_{i2n1} + N_{n2}\sigma_{i2n2})$, respectively. Here, $V_{T_e} = (2T_e/m_e)^{1/2}$ is the electron thermal speed, $\sigma_{en1}$, $\sigma_{en2}$, $\sigma_{i1n1}$, $\sigma_{i1n2}$, $\sigma_{i2n1}$, and $\sigma_{i2n2}$ are the cross sections of the electron- and ion-neutral collisions. Furthermore, $\nu_{id}^{(1)}$, $\nu_{id}^{(2)}$, and $\nu_{ed}$ are the rates of the ion/electron collection by the fine solid particles, respectively.[24,25]

In addition to the plasma species losses to the discharge walls and dispersed fine solid particles, Eqs. (1)–(3) also include volume recombination loss terms $\rho_{1e} n_{i1} n_e^2$ and $\rho_{2e} n_{i2} n_e^2$, where $\rho_{1e}$ and $\rho_{2e}$ are the three-body recombination coefficients.[26] The three-body recombination is a process in which two continuum electrons interact in the presence of the ionic field such that, as one of the electrons loses its kinetic energy and is captured, the excess energy released is carried away by the second electron.[26] Likewise, radiative recombination processes are neglected.

## III. DIFFUSION EQUILIBRIUM OF THE DISCHARGE

In the low-to-intermediate pressure range of our interest here, it is quite accurate to substitute the electric field $E$ in Eqs. (4)–(6) by the ambipolar field

$$E_{\text{amb}} = \chi^{-1}[D_{i1}\partial_x n_{i1} + D_{i2}\partial_x n_{i2} - D_e\partial_x n_e], \tag{7}$$

where $\chi = \mu_{i1} n_{i1} + \mu_{i2} n_{i2} + \mu_e n_e$ and $\partial_x \equiv \partial/\partial x$. Ambipolar fluxes of the plasma species

$$\Gamma_e = -\chi^{-1}[\mu_e n_e(D_{i1}\partial_x n_{i1} + D_{i2}\partial_x n_{i2}) + (\mu_{i1} n_{i1} + \mu_{i2} n_{i2}) D_e \partial_x n_e], \tag{8}$$

$$\Gamma_{i1} = \chi^{-1}[\mu_{i1} n_{i1}(D_{i2}\partial_x n_{i2} - D_e\partial_x n_e) - (\mu_{i2} n_{i2} + \mu_e n_e) D_{i1}\partial_x n_{i1}], \tag{9}$$

and

$$\Gamma_{i2} = \chi^{-1}[\mu_{i2} n_{i2}(D_{i1}\partial_x n_{i1} - D_e\partial_x n_e) - (\mu_{i1} n_{i1} + \mu_e n_e) D_{i2}\partial_x n_{i2}] \tag{10}$$

can be obtained by substituting Eq. (7) into Eqs. (4)–(6).[27]

The model of one-dimensional plasma column has further been simplified by introducing the notions of effective loss of the plasma species to the discharge walls,

$$\nu_{\text{wall}}^j = \left\langle \frac{1}{n_j}\frac{\partial\Gamma_j}{\partial x} \right\rangle, \tag{11}$$

where angle brackets denote spatial averaging

$$\langle\chi\rangle = L^{-1}\int_{-L/2}^{L/2} \chi(x)dx$$

over the $x$ direction and $\chi$ is the quantity being averaged. Using spatially averaged number densities of the plasma species and assuming that the rate coefficients are independent on $x$, one can obtain the following spatially averaged (also commonly termed "global"[16]) set of the particle balance equations:

$$\nu_{\text{ion}}^{\text{eff}} n_e - (\nu_{ed} + \nu_{\text{wall}}^e) n_e - (\rho_{1e} n_{i1} + \rho_{2e} n_{i2}) n_e^2 = 0, \tag{12}$$

$$\nu_{\text{ion}}^{(1)} n_e - (\nu_{id}^{(1)} + \nu_{\text{wall}}^{(i1)}) n_{i1} - \nu_{\text{ex}}^{(1)} n_{i1} + \nu_{\text{ex}}^{(2)} n_{i2} - \rho_{1e} n_{i1} n_e^2 = 0, \tag{13}$$

$$\nu_{\text{ion}}^{(2)} n_e - (\nu_{id}^{(2)} + \nu_{\text{wall}}^{(i2)}) n_{i2} - \nu_{\text{ex}}^{(2)} n_{i2} + \nu_{\text{ex}}^{(1)} n_{i1} - \rho_{2e} n_{i2} n_e^2 = 0, \tag{14}$$

where, for simplicity, spatially averaged values of number densities of the plasma species are denoted without the sign of averaging.

From Eq. (12), one obtains

$$n_e = \frac{(\nu_{\text{ion}}^{(1)} + \nu_{\text{ion}}^{(2)}) - (\nu_{ed} + \nu_{\text{wall}}^e)}{\rho_{1e} n_{i1} + \rho_{2e} n_{i2}} \tag{15}$$

for the equilibrium electron number density. From Eq. (15), it follows that the equilibrium discharge state exists if the electron creation by electron impact ionization of neutral species $n1$ and $n2$ outbalances the combined electron losses to the discharge walls and surfaces of dispersed fine solid particles. Combining Eqs. (12)–(14), we obtain

$$(\nu_{ed} + \nu_{\text{wall}}^e) n_e = (\nu_{id}^{(1)} + \nu_{\text{wall}}^{(i1)}) n_{i1} + (\nu_{id}^{(2)} + \nu_{\text{wall}}^{(i2)}) n_{i2}, \tag{16}$$

which is a diffusion equilibrium in fine particle-loaded discharge. Equation (16) generalizes previously derived complex plasma diffusion equilibrium equations[29,30] by incorporating two positive ion species and particle losses to the discharge walls. Thus, combined electron and ion losses to the discharge walls and fine particles must be balanced for the equilibrium discharge state to exist. In this case surfaces of fine particles act as dispersed microscopic walls. It is interesting to note that this conclusion is not affected by the charge exchange collisions or the three-body recombination processes in the plasma bulk.

In the following, we will assume that equal surface areas of the "real" and "microdispersed" walls collect plasma species with the same rate. The applicability of this assumption to the real situations will be discussed in Sec. V. It is notable that the effect of fine particles on plasma species losses can be appreciable only if combined surface area $4\pi\Sigma a_d^2$ of the particles is comparable with $2A_{\text{wall}} + S_{\text{lat}}$, where $A_{\text{wall}}$ is the

TABLE I. Representative ranges of dimensional parameters.

| Parameter | Notation | Value |
|---|---|---|
| Working gas pressure | $p_0$ | 20–1000 mTorr |
| Partial pressure of species 1 | $p_{01}$ | 10–500 mTorr |
| Partial pressure of species 2 | $p_{02}$ | 10–500 mTorr |
| Working positive ion mass | $m_{i1}$ | 1, 2, 12, 15, 24 amu |
| Buffer positive ion mass | $m_{i2}$ | 2, 40 amu |
| Electron temperature | $T_e$ | 1.0–15.0 eV |
| Fine solid particle size | $a_p$ | 10–100 nm |
| Temperature of neutrals 1 | $T_{n1}$ | 20–400 °C |
| Temperature of neutrals 2 | $T_{n2}$ | 20–400 °C |
| Working ion temperature | $T_{i1}$ | 0.027–0.3 eV |
| Buffer ion temperature | $T_{i2}$ | 0.027–0.3 eV |
| Working ion density ($x=0$) | $n_{i1}$ | $(0.8–8)\times10^{10}$ cm$^{-3}$ |
| Buffer ion density ($x=0$) | $n_{i2}$ | $(5–100)\times10^{9}$ cm$^{-3}$ |
| Electron density ($x=0$) | $n_e$ | $(1–18)\times10^{10}$ cm$^{-3}$ |
| Particulate density | $n_p$ | $(5–50)\times10^{6}$ cm$^{-3}$ |
| Interelectrode spacing | $L$ | 1.0–10.0 cm |
| Electrode radius | $R$ | 5–15 cm |
| Cross section of electron-neutral collisions | $\sigma_{en1}$ | $2\times10^{-15}$–$4\times10^{-15}$ cm$^2$ |
| Cross section of electron-neutral collisions | $\sigma_{en2}$ | $1.5\times10^{-15}$–$5\times10^{-15}$ cm$^2$ |
| Cross section of ion-neutral collisions | $\sigma_{i1n1}$ | $2\times10^{-15}$–$6\times10^{-14}$ cm$^2$ |
| Cross section of ion-neutral collisions | $\sigma_{i1n2}$ | $2\times10^{-15}$–$8\times10^{-14}$ cm$^2$ |
| Cross section of ion-neutral collisions | $\sigma_{i2n1}$ | $4\times10^{-15}$–$6\times10^{-14}$ cm$^2$ |
| Cross section of ion-neutral collisions | $\sigma_{i2n2}$ | $4\times10^{-15}$–$8\times10^{-14}$ cm$^2$ |
| Recombination rate constant | $\rho_{1e}$ | $10^{-17}$–$10^{-15}$ cm$^6$/s |
| Recombination rate constant | $\rho_{2e}$ | $10^{-17}$–$10^{-15}$ cm$^6$/s |
| Rate constant of charge exchange collisions | $\alpha_{\rm ex}^{(1)}$ | $(1.1–6)\times10^{-10}$ cm$^3$/s |
| Rate constant of charge exchange collisions | $\alpha_{\rm ex}^{(2)}$ | $(1–4)\times10^{-10}$ cm$^3$/s |

surface area of each of the two parallel plates limiting the plasma and $S_{\rm lat}=2\pi RL$ is the area of the lateral surface of the plasma column, where $R$ is the radius of each of the parallel plates. In this case it is reasonable to assume that a dielectric (e.g., quartz) container is brought in a reasonably close contact with conducting parallel-plate electrodes.

In this approximation, the rates of the plasma particles losses to the discharge and "dispersed" walls can be approximated as $\nu_{\rm wall}^{e}+\nu_{ed}\sim[2A_{\rm wall}+S_{\rm lat}+4\pi\Sigma a_d^2]V_{Te}n_e\times\exp(-\phi_s/T_e)$, $\nu_{\rm wall}^{(i1)}+\nu_{id}^{(1)}=[2A_{\rm wall}+S_{\rm lat}+4\pi\Sigma a_d^2]V_B^{\rm eff}n_{i1}$, and $\nu_{\rm wall}^{(i2)}+\nu_{id}^{(2)}=[2A_{\rm wall}+S_{\rm lat}+4\pi\Sigma a_d^2]V_B^{\rm eff}n_{i2}$. Here, it was assumed that both "macroscopic" and microdispersed walls have the same surface potential $\phi_s$, which is valid when the macroscopic walls are not biased externally. Otherwise, one should exercise a certain degree of caution as the introduction of two separate potentials may be in order. Furthermore,

$$V_B^{\rm eff}=[(n_{i1}/n_e)(T_e/m_{i1})+(n_{i2}/n_e)(T_e/m_{i2})]^{1/2}$$

is the effective Bohm velocity with which ion species $i1$ and $i2$ enter the sheaths surrounding the walls and the fine particles.[31]

## IV. NUMERICAL RESULTS

In this section, the set of Eqs. (12)–(14) will be investigated numerically. The range of parameters representative to typical parallel-plate discharge configurations, nanoparticle-generating complex plasmas, and process parameters of the plasma enhanced chemical vapor deposition of carbon-based nanofilms and nanostructures is presented in Table I. Most of

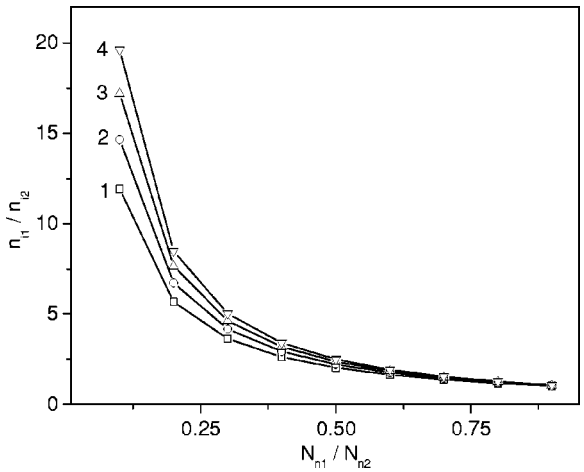


FIG. 2. Ratio of ion densities $n_{i1}/n_{i2}$ vs relative number density $N_{n1}/N_{n2}$. Curves 1–4 correspond to the following values of $\alpha_{\rm ion}^{(1)}/\alpha_{\rm ex}^{(1)}$: 0.5, 1.0, 1.5, and 2.0, respectively. Nondimensional parameters are $\alpha_{\rm ion}^{(1)}/\alpha_{\rm ion}^{(2)}=0.8$, $\alpha_{\rm ex}^{(1)}/\alpha_{\rm ex}^{(2)}=0.9$, $\nu_{\rm wall}^{(i1)}/\nu_{\rm ion}^{(1)}=0.6$, $\nu_{\rm wall}^{(i2)}/\nu_{\rm ion}^{(2)}=0.7$, $\nu_{id}^{(1)}/\nu_{\rm wall}^{(i1)}=0.125$, $\nu_{id}^{(2)}/\nu_{\rm wall}^{(i2)}=0.125$, $\rho_{1e}n_{e0}^2/\nu_{\rm wall}^{(i1)}=0.15$, and $\rho_{2e}n_{e0}^2/\nu_{\rm wall}^{(i2)}=0.15$.

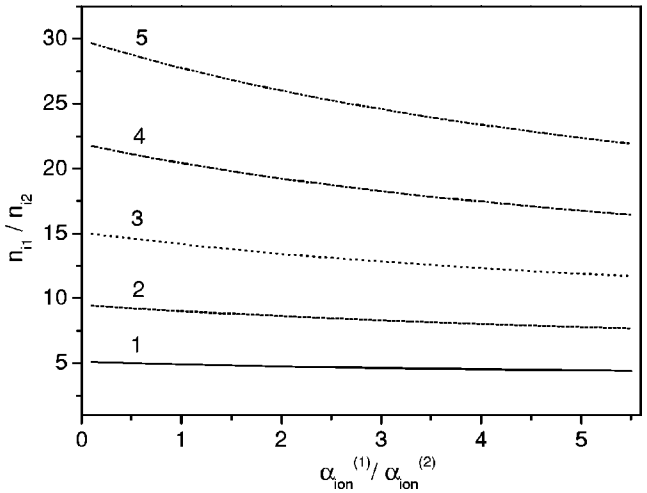


FIG. 3. Same as in Fig. 2 as a function of $\alpha_{\text{ion}}^{(1)}/\alpha_{\text{ion}}^{(2)}$. Curves 1–5 correspond to the following values of $\alpha_{\text{ex}}^{(1)}/\alpha_{\text{ex}}^{(2)}$: 0.5, 0.75, 1.0, 1.25, and 1.5, respectively. Nondimensional parameters are $N_{n1}/N_{n2}=0.15$, $\alpha_{\text{ion}}^{(1)}/\alpha_{\text{ex}}^{(1)}=2.0$. Other parameters are the same as in Fig. 2.

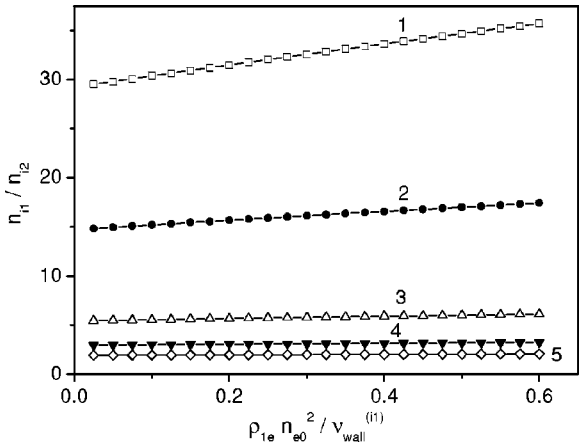


FIG. 5. Same as in Fig. 2 vs relative bulk recombination loss $\rho_{1e}n_{e0}^2/\nu_{\text{wall}}^{(i1)}$. Curves 1–5 correspond to the following values of $N_{n1}/N_{n2}$: 0.15, 0.25, 0.5, 0.75, and 1.0, respectively. Nondimensional parameters are $\nu_{\text{wall}}^{(i1)}/\nu_{\text{ion}}^{(1)}=0.6$, $\nu_{\text{wall}}^{(i2)}/\nu_{\text{ion}}^{(2)}=0.7$, $\nu_{id}^{(1)}/\nu_{\text{wall}}^{(i1)}=0.7$, $\nu_{id}^{(1)}/\nu_{\text{wall}}^{(i1)}=0.56$, and $\rho_{2e}n_{e0}^2/\nu_{\text{wall}}^{(i2)}=1.1\rho_{1e}n_{e0}^2/\nu_{\text{wall}}^{(i1)}$. Other parameters are the same as in Fig. 4.

the parameters, rate constants, etc. have been drawn from the available literature,[1–3,15,16,32–39] online databases,[40,41] and references therein. By using the parameters of Table I, a set of nondimensional parameters $N_{n1}/N_{n2}$, $\alpha_{\text{ion}}^{(1)}/\alpha_{\text{ion}}^{(2)}$, $\alpha_{\text{ex}}^{(1)}/\alpha_{\text{ex}}^{(2)}$, $\nu_{\text{wall}}^{(i1)}/\nu_{\text{ion}}^{(1)}$, $\nu_{\text{wall}}^{(i2)}/\nu_{\text{ion}}^{(2)}$, $\alpha_{\text{ion}}^{(1)}/\alpha_{\text{ex}}^{(1)}$, $\alpha_{\text{ion}}^{(2)}/\alpha_{\text{ex}}^{(2)}$, $\nu_{id}^{(1)}/\nu_{\text{wall}}^{(i1)}$, $\nu_{id}^{(2)}/\nu_{\text{wall}}^{(i2)}$, $\rho_{1e}n_{e0}^2/\nu_{\text{wall}}^{(i1)}$, and $\rho_{2e}n_{e0}^2/\nu_{\text{wall}}^{(i2)}$ was introduced and typical ranges of their variation have been worked out and used in further analysis. Parameter $N_{n1}/N_{n2}$ describes relative concentrations (partial pressures) of the two neutral species, $\alpha_{\text{ion}}^{(1)}/\alpha_{\text{ion}}^{(2)}$ is a relative rate of production of the two species $i1$ and $i2$ (at $N_{n1}/N_{n2}=1$), $\alpha_{\text{ex}}^{(1)}/\alpha_{\text{ex}}^{(2)}$ is the ratio of the charge exchange rate constants of ionic species 1 and 2, $\alpha_{\text{ion}}^{(1,2)}/\alpha_{\text{ex}}^{(1,2)}$ reflects relative importance of the species production and loss due to charge exchange collisions and electron impact ionization, $\nu_{\text{wall}}^{(i1,2)}/\nu_{\text{ion}}^{(1,2)}$ shows a proportion of species $i1$ and $i2$ (created as a result of electron impact ionization) lost to the discharge walls. Nondimensional parameters $\nu_{id}^{(1,2)}/\nu_{\text{wall}}^{(i1,2)}$ and $\rho_{(1,2)e}n_{e0}^2/\nu_{\text{wall}}^{(i1,2)}$ are indicative to relative importance of the ion loss channels to the discharge walls, fine particle surfaces, and losses due to the three-body recombination in the plasma bulk.

The set of the above nondimensional parameters has been manipulated to optimize the generation of the working species with respect to the buffer ions under conditions when charge exchange collisions control the particle balance in the discharge. Figure 2 shows the dependence of the ratio of ion number densities $n_{i1}/n_{i2}$ on the dilution factor $N_{n1}/N_{n2}$. One can see that when the ionization and charge exchange rates of both gases are comparable, and the dilution is heavy ($N_{n1}/N_{n2}<0.2$, as is quite typical in many plasma-aided nanofabrication processes) it appears possible to achieve predominant generation of the working ionic species. Different curves in Fig. 2 correspond to different values of nondimensional parameter $\alpha_{\text{ion}}^{(1)}/\alpha_{\text{ex}}^{(1)}$. When the rate of the electron impact ionization relative to that of the charge exchange collisions becomes higher, the efficiency of the $i1$ species production becomes even more efficient, as reflected by higher values of $n_{i1}/n_{i2}$ at larger $\alpha_{\text{ion}}^{(1)}/\alpha_{\text{ex}}^{(1)}$.

Figure 3 suggests that in situations when the working gas is heavily diluted in a buffer gas and charge exchange collisions are dominant, the relative number density of two ionic species $n_{i1}/n_{i2}$ can decrease with the ratio of their ionization constants $\alpha_{\text{ion}}^{(1)}/\alpha_{\text{ion}}^{(2)}$. Meanwhile, an increase of the parameter $\alpha_{\text{ex}}^{(1)}/\alpha_{\text{ex}}^{(2)}$ in three times, from 0.5 to 1.5, can cause a substantial rise (in up to five times) of $n_{i1}/n_{i2}$.

From Fig. 4, one can note that as the loss of ionic species $i1$ becomes to a larger extent controlled by the discharge walls (as formally reflected by higher $\nu_{\text{wall}}^{(1)}/\nu_{\text{ion}}^{(1)}$), the relative density of the working ionic species can be increased. Enhanced collection of the $i1$ ions by the fine solid particles (as described by higher relative collection rates $\nu_{\text{id}}^{(1)}/\nu_{\text{wall}}^{(1)}$) also appears favorable to enable predominant generation of the

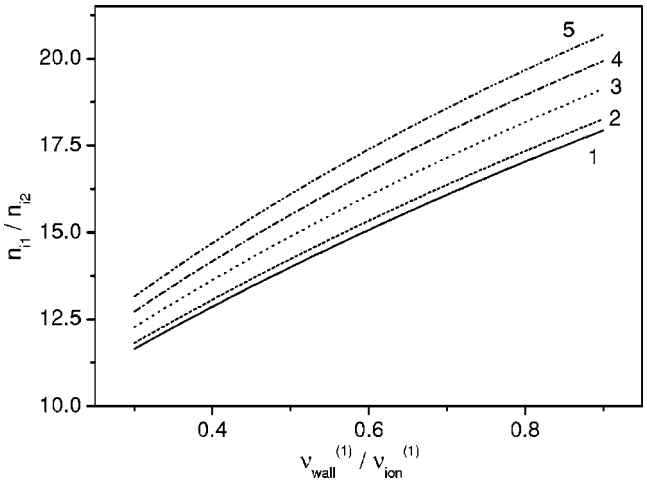


FIG. 4. Same as in Fig. 2 as a function of $\nu_{\text{wall}}^{(i1)}/\nu_{\text{ion}}^{(1)}$. Curves 1–5 correspond to the following values of $\nu_{id}^{(1)}/\nu_{\text{wall}}^{(i1)}$: 0.03, 0.1, 0.3, 0.5, and 0.7, respectively. Nondimensional parameters are $N_{n1}/N_{n2}=0.2$, $\alpha_{\text{ion}}^{(1)}/\alpha_{\text{ion}}^{(2)}=1.6$, $\alpha_{\text{ex}}^{(1)}/\alpha_{\text{ex}}^{(2)}=1.5$, $\nu_{\text{wall}}^{(i2)}/\nu_{\text{ion}}^{(2)}=0.9\nu_{\text{wall}}^{(i1)}/\nu_{\text{ion}}^{(1)}$, $\alpha_{\text{ion}}^{(1)}/\alpha_{\text{ex}}^{(1)}=2.0$, $\alpha_{\text{ion}}^{(2)}/\alpha_{\text{ex}}^{(2)}=1.875$, and $\nu_{id}^{(2)}/\nu_{\text{wall}}^{(i2)}=0.8\nu_{id}^{(1)}/\nu_{\text{wall}}^{(1)}$. Other parameters are the same as in Fig. 2.

working ion species. In the latter case, under conditions of Fig. 3, $n_{i1}/n_{i2}$ can be elevated by $\approx 15\%$–$20\%$.

Figure 5 shows a quite similar dependence of the ratio of concentrations of the ion species on the relative efficiency $\rho_{1e} n_{e0}^2/\nu_{\text{wall}}^{(1)}$ of three-body recombination losses in the plasma bulk compared to the discharge wall losses. This effect is most pronounced when the dilution degree is the highest ($N_{n1}/N_{n2}=0.15$, curve 1). The results presented in Figs. 2–5 and their implications for tailoring ionic species composition in applications will be discussed in the following section.

## V. DISCUSSION

We note that Figs. 2–5 show the dependence of relative number density of two ionic species on various nondimensional parameters, which appears to be quite different from the case when the charge exchange collisions are unimportant. It is imperative that the results shown in Figs. 2–5 should be understood in terms of a stationary balance of the plasma species creation and loss described by Eqs. (12)–(14) under conditions of dominant charge exchange collisions.

From Fig. 2, one can see that the relative number density of the two species $i1$ and $i2$ decreases with $N_{n1}/N_{n2}$ at the same ratio of the ionization $\alpha_{\text{ion}}^{(1)}$ and charge exchange $\alpha_{\text{ex}}^{(1)}$ constants of the working gas. In the absence of charge exchange collisions, one would expect $n_{i1}/n_{i2}$ to increase when the number of neutral species 1 available for ionization, becomes larger. However, under the chosen set of parameters, larger amounts of neutral species $n2$ (equivalent to lower ratios $N_{n1}/N_{n2}$ in Fig. 2) are beneficial for the enhanced production of ionic species $i1$ in charge exchange collisions, which is consistent with the results of Fig. 2. When the ionization rates become higher (at the same $N_{n1}/N_{n2}$), the efficiency of production of ionic species $i1$ increases as evidenced by the increased $n_{i1}/n_{i2}$ with $\alpha_{\text{ion}}^{(1)}/\alpha_{\text{ex}}^{(1)}$.

Figure 3 presents an even less obvious result suggesting that $n_{i1}/n_{i2}$ can decrease with $\alpha_{\text{ion}}^{(1)}/\alpha_{\text{ion}}^{(2)}$. The set of parameters (e.g., heavy dilution of the working gas in the buffer gas) has been chosen to shift the species balance towards the enhanced generation of ionic species $i1$ through the charge exchange collisions. An increase in the number of ions $i1$ due to electron impact ionization at higher $\alpha_{\text{ion}}^{(1)}/\alpha_{\text{ion}}^{(2)}$, on the other hand, causes higher loss due to charge exchange collisions with abundant neutral species $n2$, and results in somewhat lower values of $n_{i1}/n_{i2}$, as can be seen in Fig. 3. Moreover, this effect becomes more pronounced at higher $\alpha_{\text{ex}}^{(1)}/\alpha_{\text{ex}}^{(2)}$ reflecting higher efficiency of charge exchange collisions involving ionic species $i1$ and neutrals $n2$ of the buffer gas.

A somewhat similar interplay between the species creation and loss processes depicted in Fig. 4 suggests that under conditions of dominant charge exchange collisions, one can enhance production of the desired ionic species by controlling the ion loss to the walls or adding additional microdispersed walls in a form of fine solid particles. In the charge exchange collision-free environment, one would expect the ion number density to decrease when diffusion losses to the walls become stronger relative to the electron impact ionization source. However, in the heavy dilution case ($N_{n1}/N_{n2}=0.2$), a higher loss of ionic species $i1$ to the discharge walls means lower overall loss to the (dominant) charge exchange collisions, and hence, to higher concentrations of ions $i1$ with respect to that of ions $i2$, consistent with the results of Fig. 4. Addition of fine solid particles enhances this effect, as evidenced by higher $n_{i1}/n_{i2}$ for the curves with higher numbers. This can be attributed to larger combined surface areas of the discharge container and microdispersed walls at higher $\nu_{id}^{(1)}/\nu_{\text{wall}}^{(1)}$.

From the particle balance viewpoint, the effect of stronger three-body recombination losses in the plasma bulk displayed in Fig. 5 is conceptually similar to that of the fine solid component (Fig. 4, different curves). On the other hand, higher values of relative ion densities for the curves with smaller numbers can be explained similarly as the dependence $n_{i1}/n_{i2}$ on $N_{n1}/N_{n2}$ of Fig. 2.

It is notable that charge exchange collisions are essential in the theory of the effect of trapped ions on fine particle charging in complex plasmas.[22,23] Indeed, low-energy positive ions generated as a result of charge exchange collisions can be trapped by electrostatic potentials and eventually be collected by fine particles.

Thus, incorporating more specific details of the fine particle charging under conditions of dominant charge exchange collisions, such as including trapped ions, can become critical for the future development of our discharge model. Furthermore, we have assumed that equal surface areas of the macroscopic and microdispersed walls collect plasma species with the same rate. Physically, this assumption is equivalent to the case when the fine particles are large enough and collect electrons and ions from the plasma like macroscopic spherical Langmuir probes.[42] In the latter case, the plasma species are collected by the probe surfaces predominantly in the radial direction, which effectively excludes any orbital motions. Formally, the charging problem is treated by assuming fine particle charging by radial fluxes[42] rather than by orbit motion limited currents.[7]

Our model is quite simple and sidesteps many important processes in the discharge, such as power balance, electron energy distributions, multiple species and their mutual transformations as a result of numerous heavy particle collisions, etc. However, despite its apparent simplicity, the model is instrumental in revealing the unique possibility to tailor the composition of ionic species in charge exchange collision-controlled regimes. Therefore, this contribution can be regarded as a simplified generic spatially averaged model of fine particle-loaded parallel-plate discharges under conditions of dominant charge exchange collisions.

An immediate application of the above results is in the possibility to substantially elevate the number density of the working ionic species compared to that of the buffer species, by the appropriate choice of the process conditions (e.g., working gas dilution in a buffer gas) and adjustment of the key reaction rates. While the required gas composition is a matter of appropriate mass flow control of inlet gases, the issue of adjustment of the elementary reaction rates in the ionized gas phase does not seem to be straightforward. However, an efficient strategy in this regard would be to tailor the electron and ion energy distribution functions (EEDF/IEDF),

which determine the effective electron/ion temperatures, and, hence, most of the rates of the plasma species creation and loss.[43,44] To this end, comprehensive discharge models with self-consistent EEDFs/IEDFs are warranted. Preliminary results suggest that the EEDF can be efficiently "Maxwellized" from an initially Druyvestein-like EEDF by enhancing the electron/ion collection by microdispersed fine powder particles.[45,46]

The resulting models of the ionized gas systems can be suitable to simulate and optimize various industrial plasma applications, e.g., synthesis of advanced materials and plasma-aided nanofabrication of nanoscale devices. In particular, the process of the $Ar+H_2+CH_4/C_2H_2$ plasma-assisted assembly of carbon nanotip and nanopyramid microemitters[47] in low-frequency inductively coupled plasma source[48] proceeds in three main stages.[13–15] In this case, $Ar^+$ ions are used to clean and heat the deposition surface, hydrogen activates surface dangling bonds, and cations $CH_3^+$ are believed to be the main building units of carbon nanotip and nanopyramid microemitter structures.[49,50] On the other hand, carbon dimer $C_2$ plays a vital role in nanoassembly of carbon nanotube and nanowall structures, as well as ultrananocrystalline diamond.[6,51–53] It is imperative that during each process stage selective enhancement of production of certain charged or neutral species may be in order. Specifically, during the surface pretreatment stage in pure Ar plasmas, more efficient electron impact ionization of argon gas can be used to generate larger amounts of $Ar^+$ ions. During the second (surface activation) stage, when hydrogen gas is added to the discharge in argon, it is important to enhance production of hydrogen species. At this stage, heavy particle collisions, including dissociation, Penning ionization, charge exchange, etc. processes come into play.[16] Finally, selective elevation of number densities of the nanostructure building units $C_2$ and $CH_3/CH_3^+$ is required during the third, nanostructure growth process stage.

## VI. CONCLUSION

Numerous applications of low-temperature plasmas require elevated abundance of certain ionic or radical species (termed working above) that serve for specific purpose. To this end, the discharge and process parameters should be optimized to generate the required steady-state number densities of the working species. It appears that in multicomponent chemically active plasmas one can efficiently capitalize on charge exchange collisions between the ionic and neutral species that can, under certain conditions, control the plasma species balance. Our results suggest that in some cases, e.g., when a working gas is strongly diluted in a buffer gas, and some other conditions are met, it appears possible to predominantly generate the desired working ion species and obtain steady-state number densities $n_{i1}$ exceeding by one order of magnitude (10–30 times in the examples shown) the density of the ions of the buffer gas. The purpose of this work is a generic analysis of a spatially averaged model of a common parallel-plate discharge geometry and, from a broader perspective, practical recipes to achieve higher relative number densities of the working ionic species in charge exchange collision-dominated regimes of plasma discharges loaded with fine solid particles. Nonetheless, the results of this work are relevant to controlled deposition of ionic species in the $Ar+H_2+CH_4/C_2H_2$ plasma-aided nanofabrication of ordered patterns of carbon nanotip and nanopyramid microemitters for flat display panel applications. Future numerical efforts will be focused on the improvement of the discharge model by including power balance, nonuniformity of species distribution, improving the fine particle charging model, and relating the outcomes to specific industrial applications of low-temperature ionized gas systems.

## ACKNOWLEDGMENTS

This work was supported by the Australian Research Council and by the University of Sydney.

[1] G. S. Oehrlein, *Plasma Processing of Electronic Materials* (Springer, Berlin, 2003).
[2] A. Fridman and L. A. Kennedy, *Plasma Physics and Engineering* (Taylor & Francis, New York, 2004).
[3] *Dusty Plasmas: Physics, Chemistry, and Technological Impacts in Plasma Processing*, edited by A. Bouchoule (Wiley, New York, 1999).
[4] *Nanotechnology Research Directions: Vision for Nanotechnology Research and Development in the Next Decade*, edited by M. C. Roco, S. Williams, and P. Alivisatos (Kluwer Academic, Amsterdam, 1999). See also US National Nanotechnology Initiative, http://www.nano.gov
[5] C. P. Poole, Jr. and F. J. Owens, *Introduction to Nanotechnology* (Wiley, New York, 2003).
[6] V. Shchukin, N. N. Ledentsov, and D. Bimberg, *Epitaxy of Nanostructures* (Springer, Berlin, 2003).
[7] S. V. Vladimirov and K. Ostrikov, Phys. Rep. **393**, 175 (2003).
[8] N. M. Hwang and D. Y. Kim, Int. Mater. Rev. **49**, 171 (2004).
[9] K. Ostrikov, Singapore Journal of Physics **19**, 1 (2003).
[10] C. Bower, W. Zhu, S. Jin, and O. Zhou, Appl. Phys. Lett. **77**, 830 (2000).
[11] M. Chhowalla, K. B. K. Teo, C. Dukati, N. L. Rupersinghe, G. A. J. Amaratunga, A. C. Ferrari, D. Roy, J. Robertson, and W. I. Milne, J. Appl. Phys. **90**, 5308 (2001).
[12] E. I. Waldorff, A. M. Waas, P. P. Friedmann, and M. Keidar, J. Appl. Phys. **95**, 2749 (2004).
[13] I. B. Denysenko, S. Xu, P. P. Rutkevych, J. D. Long, N. A. Azarenkov, and K. Ostrikov, J. Appl. Phys. **95**, 2713 (2004).
[14] Z. L. Tsakadze, K. Ostrikov, J. D. Long, and S. Xu, Diamond Relat. Mater. **13**, 1923 (2004).
[15] Z. L. Tsakadze, K. Ostrikov, and S. Xu, Surf. Coat. Technol. **191/1**, 49 (2005).
[16] M. A. Lieberman and A. J. Lichtenberg, *Principles of Plasma Discharges and Materials Processing* (Wiley, New York, 1994).
[17] S. Amiranashvili, M. Y. Yu, and L. Stenflo, Phys. Rev. E **67**, 016408 (2003).
[18] L. Stenflo and M. Y. Yu, Phys. Plasmas **10**, 912 (2003).
[19] J. X. Ma, M. Y. Yu, X. P. Liang, J. Zheng, W. D. Liu, and C. X. Yu, Phys. Plasmas **9**, 1584 (2002).
[20] S. Amiranashvili and M. Y. Yu, Phys. Plasmas **9**, 4825 (2002).
[21] I. B. Denysenko, K. Ostrikov, S. Xu, M. Y. Yu, and C. H. Diong, J. Appl. Phys. **94**, 6097 (2003).
[22] M. Lampe, V. Gavrishchaka, G. Ganguli, and G. Joyce, Phys. Rev. Lett. **86**, 5278 (2001).
[23] M. Lampe, R. Goswami, Z. Sternovski, S. Robertson, V. Gavrishchaka, G. Ganguli, and G. Joyce, Phys. Plasmas **10**, 1500 (2003).
[24] K. N. Ostrikov, S. V. Vladimirov, M. Y. Yu, and G. E. Morfill, Phys. Rev. E **61**, 4315 (2000).
[25] K. N. Ostrikov, S. V. Vladimirov, M. Y. Yu, and G. E. Morfill, Phys. Plasmas **7**, 461 (2000).
[26] Y. Hahn, Rep. Prog. Phys. **60**, 691 (1997).
[27] Here, we use the notion of "ambipolar fluxes" as opposed to conventionally used "ambipolar diffusion" to reflect the ambipolar electric-field driven joint motion of the plasma species simultaneously controlled by the electron/ion mobility and nonuniformity of $n_e$ and $n_{i1,2}$ (Ref. 28).
[28] R. N. Franklin, J. Phys. D **36**, 826 (2003).

[29]K. Ostrikov, I. B. Denysenko, S. V. Vladimirov, S. Xu, H. Sugai, and M. Y. Yu, Phys. Rev. E **67**, 056408 (2003).
[30]S. V. Vladimirov, K. N. Ostrikov, M. Y. Yu, and G. E. Morfill, Phys. Rev. E **67**, 036406 (2003).
[31]G. D. Severn, X. Wang, E. Ko, and N. Hershkowitz, Phys. Rev. Lett. **90**, 145001 (2003).
[32]A. G. Engelhardt and A. V. Phelps, Phys. Rev. **131**, 2115 (1963).
[33]H. Chatham, D. Hils, R. Robertson, and A. C. Gallagher, J. Chem. Phys. **79**, 1301 (1983).
[34]K. Tachibana, M. Nishida, H. Harima, and Y. Urano, J. Phys. D **17**, 1727 (1984).
[35]T. Nakano, H. Toyoda, and H. Sugai, Jpn. J. Appl. Phys., Part 1 **30**, 2912 (1991).
[36]Y.-K. Kim and M. E. Rudd, Phys. Rev. A **50**, 3954 (1994).
[37]D. A. Alman, D. N. Ruzic, and J. N. Brooks, Phys. Plasmas **7**, 1421 (2000).
[38]M. Heintze, M. Magureanu, and M. Kettlitz, J. Appl. Phys. **92**, 7022 (2002).
[39]R. L. Mills, P. C. Ray, B. Dhandapani, R. M. Mayo, and J. He, J. Appl. Phys. **92**, 7008 (2002).
[40]Kinema Research and Software, http://www. kinema. com/ download.htm
[41]NIST Atomic Spectra Database, http:// physics. nist. gov/ cgi-bin/ AtData/
[42]C. M. C. Nairn, B. M. Annaratone, and J. E. Allen, Plasma Sources Sci. Technol. **7**, 478 (1998).
[43]H. Kokura and H. Sugai, Jpn. J. Appl. Phys., Part 1 **39**, 2847 (2000).
[44]K. De Bleecker, A. Bogaerts, R. Gijbels, and W. Goedheer, Phys. Rev. E **69**, 056409 (2004).
[45]I. B. Denysenko, M. Y. Yu, K. Ostrikov, and A. Smolyakov, Phys. Rev. E **70**, 046403 (2004).
[46]I. B. Denysenko, M. Y. Yu, K. Ostrikov, N. A. Azarenkov, and L. Stenflo, Phys. Plasmas **11**, 4959 (2004).
[47]Representative field emission scanning electron micrographs of the carbon nanopyramid microemitter structures (CNPMS) concerned can be found elsewhere (Refs. 14 and 15). Typical heights and widths (at half height) of the CNPMSs are 300–400 nm and 80–120 nm, respectively. Such nanostructures have been grown in plasmas of argon, hydrogen, and methane gas mixtures under low-to-intermediate working pressures (20–100 mTorr), moderate rf powers (~2 kW), variable dc bias on the substrate (from −60 to −400 V), and with or without external substrate temperature control. Recent measurements of the electron field emission currents (Ref. 14) suggest outstanding potential of the nanopyramidal and nanotip structures for the development of advanced microemitter arrays for applications in the flat panel display technology.
[48]S. Xu, K. N. Ostrikov, Y. Li, E. L. Tsakadze, and I. R. Jones, Phys. Plasmas **8**, 2549 (2001).
[49]S. Xu, *Proceedings of the 7th Asia Pacific Conference Plasma Science Technology and 17th Symposium on Plasma Science for Materials, 29 June–2 July 2004*, Fukuoka, Japan. Invited Topical Lecture I-A13, p. 483 [Thin Sol. Films (to be published)].
[50]Structural incorporation of $CH_3^+$ cations into CNSs is consistent with recent studies (Ref. 49) of chemical structure of single-crystalline carbon nanotip structures.
[51]M. S. Dresselhaus, G. Dresselhaus, and P. Eklund, *Science of Fullerenes and Carbon Nanotubes* (Academic, New York, 1996).
[52]D. M. Gruen, P. C. Redfern, D. A. Horner, P. Zapol, and L. A. Curtis, J. Phys. Chem. B **103**, 5459 (1999).
[53]It is notable that chemical structure and reactivity of the carbon dimer molecule are favorable for its efficient insertion into hexagonal patterns of graphitelike lattices that build up the walls of numerous carbon nanotube structures (Ref. 51).